Modeling and Analysis of Two-Way Relay Non-Orthogonal Multiple Access Systems

Xinwei Yue, *Student Member, IEEE,* Yuanwei Liu, *Member, IEEE,* Shaoli Kang, Arumugam Nallanathan, *Fellow, IEEE*, and Yue Chen, *Senior Member, IEEE*

***Abstract*—A two-way relay non-orthogonal multiple access (TWR-NOMA) system is investigated, where two groups of NOMA users exchange messages with the aid of one half-duplex (HD) decode-and-forward (DF) relay. Since the signal-plus-interference-to-noise ratios (SINRs) of NOMA signals mainly depend on effective successive interference cancellation (SIC) schemes, imperfect SIC (ipSIC) and perfect SIC (pSIC) are taken into account. In order to characterize the performance of TWR-NOMA systems, we first derive closed-form expressions for both exact and asymptotic outage probabilities of NOMA users' signals with ipSIC/pSIC. Based on the derived results, the diversity order and throughput of the system are examined. Then we study the ergodic rates of users' signals by providing the asymptotic analysis in high SNR regimes. Lastly, numerical simulations are provided to verify the analytical results and show that: 1) TWR-NOMA is superior to TWR-OMA in terms of outage probability in low SNR regimes; 2) Due to the impact of interference signal (IS) at the relay, error floors and throughput ceilings exist in outage probabilities and ergodic rates for TWR-NOMA, respectively; and 3) In delay-limited transmission mode, TWR-NOMA with ipSIC and pSIC have almost the same energy efficiency. However, in delay-tolerant transmission mode, TWR-NOMA with pSIC is capable of achieving larger energy efficiency compared to TWR-NOMA with ipSIC.**

***Index Terms*—Imperfect SIC, non-orthogonal multiple access (NOMA), two-way relay**

I. INTRODUCTION

With the purpose to improve system throughput and spectrum efficiency, the fifth generation (5G) mobile communication networks are receiving a great deal of attention. The requirements of 5G networks mainly contain key performance indicator (KPI) improvement and support for new radio (NR) scenarios [2], including enhanced mobile broadband (eMBB), massive machine type communications (mMTC), and ultra-reliable and low latency communications (URLLC). Apart from crux technologies, such as massive multiple-input multiple-output (MIMO), millimeter wave and heterogeneous networks, the design of novel multiple access (MA) techniques is significant to make the contributions for 5G networks. Driven by these, non-orthogonal multiple access (NOMA) has been viewed as one of promising technologies to increase system capacity and user access [3]. The basic concept of NOMA is to superpose multiple users by sharing radio resources (i.e., time/frequencey/code) over different power levels [4, 5]. Then the desired signals are detected by exploiting the successive interference cancellation (SIC) [6]. More specifically, downlink multiuser superposition (MUST) transmission [7], which is one of special case for NOMA has been researched for Long Term Evolution (LTE) in 3rd generation partnership project (3GPP) and approved as work item (WI) in radio access network (RAN) meeting.

Until now, point-to-point NOMA has been discussed extensively in many research contributions [8–11]. In [8], the authors have investigated the outage performance and ergodic rate of downlink NOMA with randomly deployed users by invoking stochastic geometry. Considering the secrecy issues of NOMA against external eavesdroppers, the authors in [9] investigated secrecy outage behaviors of NOMA in larger-scale networks for both single-antenna and multiple-antenna transmission scenarios. Explicit insights for understanding the asynchronous NOMA, a novel interference cancellation scheme was proposed in [10], where the bit error rate and throughput performance were analyzed. By the virtue of available CSI, the performance of NOMA based multicast cognitive radio scheme (MCR-NOMA) was evaluated [11], in which outage probability and diversity order are obtained for both secondary and primary networks. Very recently, the application of cooperative communication [12] to NOMA is an efficient way to offer enhanced spectrum efficiency and spatial diversity. Hence the integration of cooperative communication with NOMA has been widely discussed in many treaties [13–16]. Cooperative NOMA has been proposed in [13], where the user with better channel condition acts as a decode-and-forward (DF) relay to forward information. Furthermore, in [14], the authors studied the ergodic rate of DF relay for a NOMA system. With the objective of improving energy efficiency, the application of simultaneous wireless information and power transfer (SWIPT) to the nearby user was investigated where the locations of NOMA users were modeled by stochastic geometry [15]. Considering the impact of imperfect channel state information (CSI), the authors in [16] investigated the performance of amplify-and-forward (AF) relay for downlink NOMA networks, where the exact and tight bounds of outage probability were derived. Moreover, in [17], the outage behavior and ergodic sum rate of NOMA for AF relay was analyzed under Nakagami-m fading channels. To further enhance spectrum efficiency, the performance of full-duplex (FD) cooperative NOMA was characterized in terms

X. Yue and S. Kang are with School of Electronic and Information Engineering, Beihang university, Beijing, China. S. Kang is also with State Key Laboratory of Wireless Mobile Communications, China Academy of Telecommunication Technology(CATT), Beijing, China (email: xinwei_yue@buaa.edu.cn, kangshaoli@catt.cn).

Y. Liu, A. Nallanathan and Y. Chen are with School of Electronic Engineering and Computer Science, Queen Mary University of London, London, UK (email: {yuanwei.liu, a.nallanathan and yue.chen}@qmul.ac.uk). Part of this work has been submitted to IEEE ICC 2018 [1].

of outage probability [18].

Above existing treaties on cooperative NOMA are all based on one-way relay scheme, where the messages are delivered in only one direction, (i.e., from the BS to the relay or user destinations). As a further advance, two-way relay (TWR) technique introduced in [19] has attracted remarkable interest as it is capable of boosting spectral efficiency. The basic idea of TWR systems is to exchange information between two nodes with the help of a relay, where AF or DF protocol can be employed. With the emphasis on user selection, in [20], the authors analyzed the performance of multi-user TWR channels for half-duplex (HD) AF relays. By applying physical-layer network coding (PNC) schemes, the performance of two-way AF relay systems was investigated in terms of outage probability and sum rate [21]. It was shown that two time slots PNC scheme achieves a higher sum rate compared to four time slot transmission mode. In [22], the authors studied the outage behaviors of DF relay with perfect and imperfect CSI conditions, where a new relay selection scheme was proposed to reduce the complexity of TWR systems. In terms of CSI and system state information, the system outage behavior was investigated for two-way full-duplex (FD) DF relay on different multi-user scheduling schemes [23]. In [24], the authors investigated the performance of multi-antenna TWR networks in which both AF and DF protocols are examined, respectively. Taking residual self-interference into account, the tradeoffs between the outage probability and ergodic rate were analyzed in [25] for FD TWR systems. In addition, the authors in [26] studied the performance of cooperative spectrum sharing by utilizing TWR over general fading channels. It was worth mentioning that the effective spectrum sharing is achieved by restraining additional cooperative diversity order.

A. Motivations and Contributions

While the aforementioned theoretical researches have laid a solid foundation for the understanding of NOMA and TWR techniques in wireless networks, the TWR-NOMA systems are far from being well understood. Obviously, the application of TWR to NOMA is a possible approach to improve the spectral efficiency of systems. To the best of our knowledge, there is no contributions to investigate the performance of TWR for NOMA systems. Moreover, the above contributions for NOMA have been comprehensively studied under the assumption of perfect SIC (pSIC). In practical scenarios, there still exist several potential implementation issues with the use of SIC (i.e., complexity scaling and error propagation). More precisely, these unfavorable factors will lead to errors in decoding. Once an error occurs for carrying out SIC at the nearby user, the NOMA systems will suffer from the residual interference signal (IS). Hence it is significant to examine the detrimental impacts of imperfect SIC (ipSIC) for TWR-NOMA. Motivated by these, we investigate the performance of TWR-NOMA with ipSIC/pSIC in terms of outage probability, ergodic rate and energy efficiency, where two groups of NOMA users exchange messages with the aid of a relay node using DF protocol.

The essential contributions of our paper are summarized as follows:

1) We derive the closed-form expressions of outage probability for TWR-NOMA with ipSIC/pSIC. Based on the analytical results, we further derive the corresponding asymptotic outage probabilities and obtain the diversity orders. Additionally, we discuss the system throughput in delay-limited transmission mode.
2) We show that the outage performance of TWR-NOMA is superior to TWR-OMA in the low signal-to-noise ratio (SNR) regime. We observe that due to the effect of IS at the relay, the outage probabilities for TWR-NOMA converge to error floors in the high SNR regime. We confirm that the use of pSIC is incapable of overcoming the zero diversity order for TWR-NOMA.
3) We study the ergodic rate of users' signals for TWR-NOMA with ipSIC/pSIC. To gain more insights, we discuss one special case that when there is no IS between a pair of antennas at the relay. On the basis of results derived, we obtain the zero high SNR slopes for TWR-NOMA systems. We demonstrate that the ergodic rates for TWR-NOMA converge to throughput ceilings in high SNR regimes.
4) We analyze the energy efficiency of TWR-NOMA with ipSIC/pSIC in both the delay-limited and tolerant transmission modes. We confirm that TWR-NOMA with ipSIC/pSIC in delay-limited transmission mode has almost the same energy efficiency. Furthermore, in delay-tolerant transmission mode, the energy efficiency of system with pSIC is higher than that of system with ipSIC.

B. Organization and Notation

The remainder of this paper is organised as follows. In Section II, the system mode for TWR-NOMA is introduced. In Section III, the analytical expressions for outage probability, diversity order and system throughput of TWR-NOMA are derived. Then the ergodic rates of users' signals for TWR-NOMA are investigated in Section IV. The system energy efficiency is evaluated in Section V. Analytical results and numerical simulations are presented in Section VI, which is followed by our conclusions in Section VII.

The main notations of this paper is shown as follows: $\mathbb{E}\{\cdot\}$ denotes expectation operation; $f_X(\cdot)$ and $F_X(\cdot)$ denote the probability density function (PDF) and the cumulative distribution function (CDF) of a random variable X.

II. System Model

A. System Description

We focus our attentions on a two-way relay NOMA communication scenario which consists of one relay R, two pairs of NOMA users $G_1 = \{D_1, D_2\}$ and $G_2 = \{D_3, D_4\}$[1]. To reduce the complexity of systems, many research contributions on NOMA have been proposed to pair two users for the

[1]The geographical dimensions of clusters G_1 and G_2 are to ensure that there is a certain distance difference from distant user and nearby user to R.

application of NOMA protocol[2] [27, 28]. As shown in Fig. 1, we assume that D_1 and D_3 are the nearby users in groups G_1 and G_2, respectively, while D_2 and D_4 are the distant users in groups G_1 and G_2, respectively. It is worth noting that the nearby user and distant user are distinguished based on the distance from the users to R [29]. For example, D_1 and D_3 are near to R, while D_2 and D_4 are far away from R. The exchange of information between user groups G_1 and G_2 is facilitated via the assistance of a decode-and-forward (DF) relay with two antennas, namely A_1 and A_2[3]. User nodes are equipped with single antenna and transmit the signals by utilizing superposition coding scheme. In practical communication process, the complexity of DF protocol is too high to implement. To facilitate analysis, we focus our attention on a idealized DF protocol, where R is capable of decoding the users' information correctly. Relaxing this idealized assumption can make system mode close to the practical scenario, but this is beyond the scope of this treatise. Additionally, to evaluate the impact of error propagation on TWR-NOMA, ipSIC operation is employed at relay R and nearby users. It is assumed that the direct links between two pairs of users are inexistent due to the effect of strong shadowing. Without loss of generality, all the wireless channels are modeled to be independent quasi-static block Rayleigh fading channels and disturbed by additive white Gaussian noise with mean power N_0. Furthermore, h_1, h_2, h_3 and h_4 are denoted as the complex channel coefficient of $D_1 \leftrightarrow R$, $D_2 \leftrightarrow R$, $D_3 \leftrightarrow R$ and $D_4 \leftrightarrow R$ links, respectively. We assume that the channels from user nodes to R and the channels from R to user nodes are reciprocal. In other words, the channels from user nodes to R have the same fading impact as the channels from R to the user nodes [25, 30, 31]. The channel power gains $|h_1|^2$, $|h_2|^2$, $|h_3|^2$ and $|h_4|^2$ are assumed to be exponentially distributed random variables (RVs) with the parameters Ω_i, $i \in \{1, 2, 3, 4\}$, respectively. Note that the perfect CSIs of NOMA users are available at R for signal detection.

B. Signal Model

During the first slot, the pair of NOMA users in G_1 transmit the signals to R just as uplink NOMA. Since R is equipped with two antennas, when R receives the signals from the pair of users in G_1, it will suffer from interference signals from the pair of users in G_2. More precisely, the observation at R for A_1 is given by

$$y_{R_{A_1}} = h_1\sqrt{a_1 P_u}x_1 + h_2\sqrt{a_2 P_u}x_2 + \varpi_1 I_{R_{A_2}} + n_{R_{A_1}}, \tag{1}$$

where $I_{R_{A_2}}$ denotes IS from A_2 with $I_{R_{A_2}} = (h_3\sqrt{a_3 P_u}x_3 + h_4\sqrt{a_4 P_u}x_4)$. $\varpi_1 \in [0, 1]$ denotes the impact levels of IS at R. P_u is the transmission power at user nodes. x_1, x_2 and x_3, x_4 are the signals of D_1, D_2 and D_3, D_4, respectively, i.e, $\mathbb{E}\{x_1^2\} = \mathbb{E}\{x_2^2\} = \mathbb{E}\{x_3^2\} = \mathbb{E}\{x_4^2\} = 1$. a_1, a_2 and a_3, a_4 are the corresponding power allocation coefficients. Note that the efficient uplink power control is capable of enhancing the performance of the systems considered, which is beyond the scope of this paper. $n_{R_{A_j}}$ denotes the Gaussian noise at R for A_j, $j \in \{1, 2\}$.

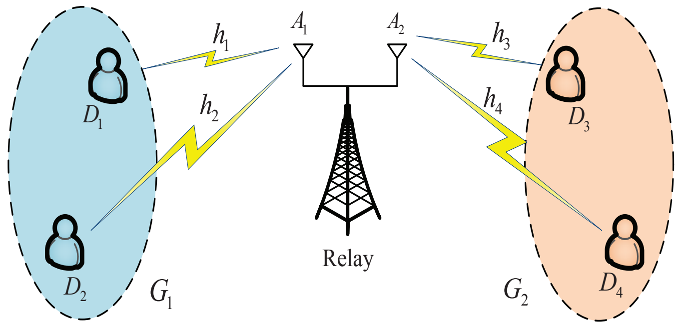

Fig. 1: An illustration of TWR-NOMA systems, in which two groups of users exchange messages with the aid of one relay node.

Similarly, when R receives the signals from the pair of users in G_2, it will suffer from interference signals from the pair of users in G_1 as well and then the observation at R is given by

$$y_{R_{A_2}} = h_3\sqrt{a_3 P_u}x_3 + h_4\sqrt{a_4 P_u}x_4 + \varpi_1 I_{R_{A_1}} + n_{R_{A_2}}, \tag{2}$$

where $I_{R_{A_1}}$ denotes the interference signals from A_1 with $I_{R_{A_1}} = (h_1\sqrt{a_1 P_u}x_1 + h_2\sqrt{a_2 P_u}x_2)$.

Applying the NOMA protocol, R first decodes D_l's information x_l by the virtue of treating x_t as IS. Hence the received signal-to-interference-plus-noise ratio (SINR) at R to detect x_l is given by

$$\gamma_{R\to x_l} = \frac{\rho |h_l|^2 a_l}{\rho |h_t|^2 a_t + \rho\varpi_1(|h_k|^2 a_k + |h_r|^2 a_r) + 1}, \tag{3}$$

where $\rho = \frac{P_u}{N_0}$ denotes the transmit signal-to-noise ratio (SNR), $(l, k) \in \{(1, 3), (3, 1)\}$, $(t, r) \in \{(2, 4), (4, 2)\}$.

After SIC is carried out at R for detecting x_l, the received SINR at R to detect x_t is given by

$$\gamma_{R\to x_t} = \frac{\rho |h_t|^2 a_t}{\varepsilon\rho |g|^2 + \rho\varpi_1(|h_k|^2 a_k + |h_r|^2 a_r) + 1}, \tag{4}$$

where $\varepsilon = 0$ and $\varepsilon = 1$ denote the pSIC and ipSIC employed at R, respectively. Due to the impact of ipSIC, the residual IS is modeled as Rayleigh fading channels [32] denoted as g with zero mean and variance Ω_I.

In the second slot, the information is exchanged between G_1 and G_2 by the virtue of R. Therefore, just like the downlink NOMA, R transmits the superposed signals $(\sqrt{b_1 P_r}x_1 + \sqrt{b_2 P_r}x_2)$ and $(\sqrt{b_3 P_r}x_3 + \sqrt{b_4 P_r}x_4)$ to G_2 and G_1 by A_2 and A_1, respectively. b_1 and b_2 denote the power allocation coefficients of D_1 and D_2, while b_3 and b_4 are the corresponding power allocation coefficients of D_3 and D_4, respectively. P_r is the transmission power at R and we assume $P_u = P_r$. In particular, to ensure the fairness between

[2] Note that increasing the number of paired users, i,e,. N pairs of users, will not affect the performance of TWR-NOMA system. It is worth pointing that within each group, superposition coding and SIC are employed, and across the groups, transmissions are orthogonal.

[3] For the practical scenario, we can assume that the relay is located on a mountain, where the user nodes on both sides of the mountain are capable of exchanging the information between each other.

users in G_1 and G_2, a higher power should be allocated to the distant user who has the worse channel condition. Hence we assume that $b_2 > b_1$ with $b_1 + b_2 = 1$ and $b_4 > b_3$ with $b_3 + b_4 = 1$. Note that the fixed power allocation coefficients for two groups' NOMA users are considered. Relaxing this assumption will further improve the performance of systems and should be concluded in our future work.

According to NOMA protocol, SIC is employed and the received SINR at D_k to detect x_t is given by

$$\gamma_{D_k \to x_t} = \frac{\rho |h_k|^2 b_t}{\rho |h_k|^2 b_l + \rho \varpi_2 |h_k|^2 + 1}, \tag{5}$$

where $\varpi_2 \in [0,1]$ denotes the impact level of IS at the user nodes. Then D_k detects x_l and gives the corresponding SINR as follows:

$$\gamma_{D_k \to x_l} = \frac{\rho |h_k|^2 b_l}{\varepsilon \rho |g|^2 + \rho \varpi_2 |h_k|^2 + 1}. \tag{6}$$

Furthermore, the received SINR at D_t to detect x_r can be given by

$$\gamma_{D_r \to x_t} = \frac{\rho |h_r|^2 b_t}{\rho |h_r|^2 b_l + \rho \varpi_2 |h_r|^2 + 1}. \tag{7}$$

From above process, the exchange of information is achieved between the NOMA users for G_1 and G_2. More specifically, the signal x_1 of D_1 is exchanged with the signal x_3 of D_3. Furthermore, the signal x_2 of D_2 is exchanged with the signal x_4 of D_4.

III. Outage Probability

In this section, the performance of TWR-NOMA is characterized in terms of outage probability. Due to the channel's reciprocity, the outage probability of x_l and x_t are provided in detail in the following part.

1) Outage Probability of x_l: In TWR-NOMA system, the outage events of x_l are explained as: i) R cannot decode x_l correctly; ii) The information x_t cannot be detected by D_k; and iii) D_k cannot detect x_l, while D_k can first decode x_t successfully. To simplify the analysis, the complementary events of x_l are employed to express its outage probability. As a consequence, the outage probability of x_l with ipSIC for TWR-NOMA system can be given by

$$\begin{aligned} P_{x_l}^{ipSIC} =& 1 - \Pr\left(\gamma_{R \to x_l} > \gamma_{th_l}\right) \\ & \times \Pr\left(\gamma_{D_k \to x_t} > \gamma_{th_t}, \gamma_{D_k \to x_l} > \gamma_{th_l}\right), \end{aligned} \tag{8}$$

where $\varepsilon = 1$, $\varpi_1 \in [0,1]$ and $\varpi_2 \in [0,1]$. $\gamma_{th_l} = 2^{2R_l} - 1$ with R_l being the target rate at D_k to detect x_l and $\gamma_{th_t} = 2^{2R_t} - 1$ with R_t being the target rate at D_k to detect x_t.

The following theorem provides the outage probability of x_l for TWR-NOMA.

Theorem 1. *The closed-form expression for the outage probability of x_l for TWR-NOMA with ipSIC is given by*

$$\begin{aligned} P_{x_l}^{ipSIC} =& 1 - e^{-\frac{\beta_l}{\Omega_l}} \prod_{i=1}^{3} \lambda_i \left(\frac{\Phi_1 \Omega_l}{\Omega_l \lambda_1 + \beta_l} - \frac{\Phi_2 \Omega_l}{\Omega_l \lambda_2 + \beta_l} \right. \\ & \left. + \frac{\Phi_3 \Omega_l}{\Omega_l \lambda_3 + \beta_l} \right) \left(e^{-\frac{\theta_l}{\Omega_k}} - \frac{\varepsilon \tau_l \rho \Omega_I}{\Omega_k + \varepsilon \rho \tau_l \Omega_I} e^{-\frac{\theta_l \left(\Omega_k + \varepsilon \rho \tau_l \Omega_I\right)}{\varepsilon \tau_l \rho \Omega_I \Omega_k} + \frac{1}{\varepsilon \rho \Omega_I}} \right), \end{aligned} \tag{9}$$

where $\varepsilon = 1$. $\lambda_1 = \frac{1}{\rho a_t \Omega_t}$, $\lambda_2 = \frac{1}{\rho \varpi_1 a_k \Omega_k}$ and $\lambda_3 = \frac{1}{\rho \varpi_1 a_r \Omega_r}$. $\beta_l = \frac{\gamma_{th_l}}{\rho a_l}$. $\Phi_1 = \frac{1}{(\lambda_2 - \lambda_1)(\lambda_3 - \lambda_1)}$, $\Phi_2 = \frac{1}{(\lambda_3 - \lambda_2)(\lambda_2 - \lambda_1)}$ and $\Phi_3 = \frac{1}{(\lambda_3 - \lambda_1)(\lambda_3 - \lambda_2)}$. $\theta_l \triangleq \max(\tau_l, \xi_t)$. $\tau_l = \frac{\gamma_{th_l}}{\rho \left(b_l - \varpi_2 \gamma_{th_l}\right)}$ with $b_l > \varpi_2 \gamma_{th_l}$ and $\xi_t = \frac{\gamma_{th_t}}{\rho \left(b_t - b_l \gamma_{th_t} - \varpi_2 \gamma_{th_t}\right)}$ with $b_t > (b_l + \varpi_2) \gamma_{th_t}$.

Proof: See Appendix A. ■

Corollary 1. *Based on (9), for the special case $\varepsilon = 0$, the outage probability of x_1 for TWR-NOMA with pSIC is given by*

$$\begin{aligned} P_{x_l}^{pSIC} =& 1 - e^{-\frac{\beta_l}{\Omega_l} - \frac{\theta_l}{\Omega_k}} \prod_{i=1}^{3} \lambda_i \left(\frac{\Phi_1 \Omega_l}{\Omega_l \lambda_1 + \beta_l} - \frac{\Phi_2 \Omega_l}{\Omega_l \lambda_2 + \beta_l} \right. \\ & \left. + \frac{\Phi_3 \Omega_l}{\Omega_l \lambda_3 + \beta_l} \right). \end{aligned} \tag{10}$$

2) Outage Probability of x_t: Based on NOMA principle, the complementary events of outage for x_t have the following cases. One of the cases is that R can first decode the information x_l and then detect x_t. Another case is that either of D_k and D_r can detect x_t successfully. Hence the outage probability of x_t can be expressed as

$$\begin{aligned} P_{x_t}^{ipSIC} =& 1 - \Pr\left(\gamma_{R \to x_t} > \gamma_{th_t}, \gamma_{R \to x_l} > \gamma_{th_l}\right) \\ & \times \Pr\left(\gamma_{D_k \to x_t} > \gamma_{th_t}\right) \Pr\left(\gamma_{D_r \to x_t} > \gamma_{th_t}\right), \end{aligned} \tag{11}$$

where $\varepsilon = 1$, $\varpi_1 \in [0,1]$ and $\varpi_2 \in [0,1]$.

The following theorem provides the outage probability of x_t for TWR-NOMA.

Theorem 2. *The closed-form expression for the outage probability of x_t with ipSIC is given by*

$$\begin{aligned} P_{x_t}^{ipSIC} =& 1 - \frac{e^{-\frac{\beta_l}{\Omega_l} - \beta_t \varphi_t - \frac{\xi}{\Omega_k} - \frac{\xi}{\Omega_r}}}{\varphi_t \Omega_t \left(1 + \varepsilon \beta_t \rho \varphi_t \Omega_I\right) \left(\lambda_2' - \lambda_1'\right)} \prod_{i=1}^{2} \lambda_i' \\ & \times \left(\frac{\Omega_l}{\beta_l + \beta_t \Omega_l \varphi_t + \Omega_l \lambda_1'} - \frac{\Omega_l}{\beta_l + \beta_t \Omega_l \varphi_t + \Omega_l \lambda_2'} \right), \end{aligned} \tag{12}$$

where $\varepsilon = 1$. $\lambda_1' = \frac{1}{\rho \varpi_1 a_k \Omega_k}$ and $\lambda_2' = \frac{1}{\rho \varpi_1 a_r \Omega_r}$. $\beta_t = \frac{\gamma_{th_t}}{\rho a_t}$, $\varphi_t = \frac{\Omega_l + \rho \beta_l a_t \Omega_t}{\Omega_l \Omega_t}$.

Proof: See Appendix B. ■

Corollary 2. *For the special case, substituting $\varepsilon = 0$ into (12), the outage probability of x_2 for TWR-NOMA with pSIC is given by*

$$\begin{aligned} P_{x_t}^{pSIC} =& 1 - \frac{e^{-\frac{\beta_l}{\Omega_l} - \beta_t \varphi_t - \frac{\xi}{\Omega_k} - \frac{\xi}{\Omega_r}}}{\varphi_t \Omega_t \left(\lambda_2' - \lambda_1'\right)} \prod_{i=1}^{2} \lambda_i' \\ & \times \left(\frac{\Omega_l}{\beta_l + \beta_t \Omega_l \varphi_t + \Omega_l \lambda_1'} - \frac{\Omega_l}{\beta_l + \beta_t \Omega_l \varphi_t + \Omega_l \lambda_2'} \right). \end{aligned} \tag{13}$$

3) Diversity Order Analysis: In order to gain deeper insights for TWR-NOMA systems, the asymptotic analysis are presented in high SNR regimes based on the derived outage probabilities. The diversity order is defined as [33]

$$d = -\lim_{\rho \to \infty} \frac{\log\left(P_{x_i}^{\infty}(\rho)\right)}{\log \rho}, \tag{14}$$

where $P_{x_i}^{\infty}$ denotes the asymptotic outage probability of x_i.

Proposition 1. *Based on the analytical results in* (9) *and* (10)*, when $\rho \to \infty$, the asymptotic outage probabilities of x_l for ipSIC/pSIC with $e^{-x} \approx 1-x$ are given by*

$$P_{x_l,\infty}^{ipSIC} = 1 - \prod_{i=1}^{3} \lambda_i \left(\frac{\Phi_1 \Omega_l}{\Omega_l \lambda_1 + \beta_l} - \frac{\Phi_2 \Omega_l}{\Omega_l \lambda_2 + \beta_l} + \frac{\Phi_3 \Omega_l}{\Omega_l \lambda_3 + \beta_l} \right) \times \left[1 - \frac{\theta_l}{\Omega_k} - \frac{\varepsilon \tau_l \rho \Omega_I}{\Omega_k + \varepsilon \rho \tau_l \Omega_I} \left(1 - \frac{\theta_l \left(\Omega_k + \varepsilon \tau_l \rho \Omega_I \right)}{\varepsilon \rho \tau_l \Omega_I \Omega_k} \right) \right], \tag{15}$$

and

$$P_{x_l,\infty}^{pSIC} = 1 - \prod_{i=1}^{3} \lambda_i \left(\frac{\Phi_1 \Omega_l}{\Omega_l \lambda_1 + \beta_l} - \frac{\Phi_2 \Omega_l}{\Omega_l \lambda_2 + \beta_l} + \frac{\Phi_3 \Omega_l}{\Omega_l \lambda_3 + \beta_l} \right), \tag{16}$$

respectively. Substituting (15) *and* (16) *into* (14)*, the diversity orders of x_l with ipSIC/pSIC are equal to zeros.*

Remark 1. *An important conclusion from above analysis is that due to impact of residual interference, the diversity order of x_l with the use of ipSIC is zero. Additionally, the communication process of the first slot similar to uplink NOMA, even though under the condition of pSIC, diversity order is equal to zero as well for x_l. As can be observed that there are error floors for x_l with ipSIC/pSIC.*

Proposition 2. *Similar to the resolving process of x_l, the asymptotic outage probabilities of x_t with ipSIC/pSIC in high SNR regimes are given by*

$$P_{x_t,\infty}^{ipSIC} = 1 - \frac{\lambda_1^{'} \lambda_2^{'}}{\varphi_t \Omega_t \left(1 + \varepsilon \rho \beta_t \varphi_t \Omega_I\right) \left(\lambda_2^{'} - \lambda_1^{'}\right)} \times \left(\frac{\Omega_l}{\beta_l + \beta_t \Omega_1 \varphi_t + \Omega_l \lambda_1^{'}} - \frac{\Omega_l}{\beta_l + \beta_t \Omega_1 \varphi_t + \Omega_l \lambda_2^{'}} \right), \tag{17}$$

and

$$P_{x_t,\infty}^{pSIC} = 1 - \frac{\lambda_1^{'} \lambda_2^{'}}{\varphi_t \Omega_t \left(\lambda_2^{'} - \lambda_1^{'}\right)} \times \left(\frac{\Omega_l}{\beta_l + \beta_t \Omega_1 \varphi_t + \Omega_l \lambda_1^{'}} - \frac{\Omega_l}{\beta_l + \beta_t \Omega_l \varphi_t + \Omega_l \lambda_2^{'}} \right), \tag{18}$$

respectively. Substituting (17) *and* (18) *into* (14)*, the diversity orders of x_t for both ipSIC and pSIC are zeros.*

Remark 2. *Based on above analytical results of x_l, the diversity orders of x_t with ipSIC/pSIC are also equal to zeros. This is because residual interference is existent in the total communication process.*

4) Throughput Analysis: In delay-limited transmission scenario, the BS transmits message to users at a fixed rate, where system throughput will be subject to wireless fading channels. Hence the corresponding throughput of TWR-NOMA with ipSIC/pSIC is calculated as [15, 34]

$$R_{dl}^{\psi} = \left(1 - P_{x_1}^{\psi}\right) R_{x_1} + \left(1 - P_{x_2}^{\psi}\right) R_{x_2} + \left(1 - P_{x_3}^{\psi}\right) R_{x_3} + \left(1 - P_{x_4}^{\psi}\right) R_{x_4}, \tag{19}$$

where $\psi \in (ipSIC, pSIC)$. $P_{x_1}^{\psi}$ and $P_{x_3}^{\psi}$ with ipSIC/pSIC can be obtained from (9) and (10), respectively, while $P_{x_2}^{\psi}$ and $P_{x_4}^{\psi}$ with ipSIC/pSIC can be obtained from (12) and (13), respectively.

IV. Ergodic Rate

In this section, the ergodic rate of TWR-NOMA is investigated for considering the influence of signal's channel fading to target rate.

1) Ergodic Rate of x_l: Since x_l can be detected at the relay as well as at D_k successfully. By the virtue of (3) and (6), the achievable rate of x_l for TWR-NOMA is written as $R_{x_l} = \frac{1}{2} \log \left(1 + \min \left(\gamma_{R \to x_l}, \gamma_{D_k \to x_l}\right)\right)$. In order to further calculate the ergodic rate of x_l, using $X = \min \left(\gamma_{R \to x_l}, \gamma_{D_k \to x_l}\right)$, the corresponding CDF F_X is presented in the following lemma.

Lemma 1. *The CDF F_X for x_l is given by* (20) *at the top of the next page, where $f_W(w) = \frac{\tilde{\lambda}_1 \tilde{\lambda}_2}{\tilde{\lambda}_2 - \tilde{\lambda}_1} \left(e^{-\tilde{\lambda}_1 w} - e^{-\tilde{\lambda}_2 w} \right)$ and $f_Z(z) = \prod_{i=1}^{3} \lambda_i \left(\Phi_1 e^{-\lambda_1 z} - \Phi_2 e^{-\lambda_2 z} + \Phi_3 e^{-\lambda_3 z} \right)$, $\tilde{\lambda}_1 = \frac{1}{\varepsilon \rho}$, $\tilde{\lambda}_2 = \frac{1}{\rho \varpi_2}$. $\varphi = \frac{a_l (w+1) \Omega_l + b_l (z+1) \Omega_k}{a_l (w+1) \Omega_l \Omega_k}$ and $\vartheta = \frac{a_l (w+1) \Omega_l + b_l (z+1) \Omega_k}{b_l (z+1) \Omega_k \Omega_l}$.*

Proof: See Appendix C. ■

Substituting (20), the corresponding ergodic rate of x_l is given by

$$R_{x_l}^{erg} = \frac{1}{2 \ln 2} \int_0^{\infty} \frac{1 - F_X(x)}{1 + x} dx, \tag{21}$$

where $X = \min \left(\gamma_{R \to x_l}, \gamma_{D_k \to x_l}\right)$ and $\varepsilon = 1$. Unfortunately, it is difficult to obtain the closed-form expression from (21). However, it can be evaluated by applying numerical approaches. To further obtain analytical results, we consider the special cases of x_l with ipSIC/pSIC for TWR-NOMA where there is no IS between the pair of antennas at the relay in the following part.

Based on the above analysis, for the special case that substituting $\varpi_1 = \varpi_2 = 0$ into (21), the ergodic rate of x_l with ipSIC can be obtained in the following theorem.

Theorem 3. *The closed-form expression of ergodic rate for x_1 with ipSIC for TWR-NOMA is given by*

$$R_{x_l,erg}^{ipSIC} = \frac{-1}{2 \ln 2} \left[A e^{\Psi} \mathrm{Ei}(-\Psi) + \frac{B e^{\frac{\Psi}{\Lambda_1}}}{\Lambda_1} \mathrm{Ei}\left(\frac{-\Psi}{\Lambda_1} \right) + \frac{C e^{\frac{\Psi}{\Lambda_2}}}{\Lambda_2} \mathrm{Ei}\left(\frac{-\Psi}{\Lambda_2} \right) \right], \tag{22}$$

where $\Lambda_1 = \frac{\varepsilon \Omega_I}{b_l \Omega_k}$, $\Lambda_2 = \frac{a_t \Omega_t}{a_l \Omega_l}$ and $\Psi = \frac{a_l \Omega_l + b_l \Omega_k}{\rho a_l b_l \Omega_l \Omega_k}$; $A = \frac{1}{\Lambda_1 \Lambda_2 - \Lambda_2 - \Lambda_1 + 1}$, $B = \frac{A(\Lambda_1 - \Lambda_1 \Lambda_2) - \Lambda_1}{(\Lambda_2 - \Lambda_1)}$ and $C = 1 - A - B$. $\mathrm{Ei}(\cdot)$ is the exponential integral function [35, Eq. (8.211.1)].

Proof: See Appendix D. ■

Corollary 3. *Based on* (22)*, the ergodic rate of x_l for pSIC with $\varepsilon = 0$ can be expressed in the closed form as*

$$R_{x_l,erg}^{pSIC} = \frac{-1}{2 \ln 2} \left[A e^{\Psi} \mathrm{Ei}(-\Psi) + \frac{C e^{\frac{\Psi}{\Lambda_2}}}{\Lambda_2} \mathrm{Ei}\left(-\frac{\Psi}{\Lambda_2} \right) \right]. \tag{23}$$

2) Ergodic Rate of x_t: On the condition that the relay and D_l are capable of detecting x_t, x_t can be also detected by D_t successfully. As a consequence, combining (4), (5) and (7), the achievable rate of x_t is written as $R_{x_t} =$

$$F_X(x) = \int_0^\infty \int_0^\infty \frac{f_W(w) f_Z(z)}{\varphi \Omega_k} \left(1 - e^{-\frac{x(w+1)\varphi}{\rho b_l}}\right) dz dw + \int_0^\infty \int_0^\infty \frac{f_W(w) f_Z(z)}{\vartheta \Omega_l} \left(1 - e^{-\frac{x(z+1)\vartheta}{\rho a_l}}\right) dz dw. \tag{20}$$

$\frac{1}{2}\log\left(1+\min\left(\gamma_{R\to x_t}, \gamma_{D_k\to x_t}, \gamma_{D_r\to x_t}\right)\right)$. The corresponding ergodic rate of x_t can be expressed as

$$R_{x_t}^{erg} = \frac{1}{2\ln 2}\int_0^\infty \frac{1-F_Y(y)}{1+y}dy, \tag{24}$$

where $Y = \min\left(\gamma_{R\to x_t}, \gamma_{D_k\to x_t}, \gamma_{D_r\to x_t}\right)$ with $\varpi_1 = \varpi_2 = 1$ and $\varepsilon = 1$. To the best of authors' knowledge, (24) does not have a closed form solution. We also consider the special cases of x_t by the virtue of ignoring IS between the pair of antennas at the relay.

For the special case that substituting $\varpi_1 = \varpi_2 = 0$ into (24) and after some manipulations, the ergodic rates of x_t with ipSIC/pSIC is given by

$$R_{x_t,erg}^{ipSIC} = \frac{1}{2\ln 2}\int_0^{\frac{b_t}{b_l}} \frac{e^{-\frac{x}{\rho a_t \Omega_t} - \frac{x}{\rho(b_t - x b_l)\Omega_k} - \frac{x}{\rho(b_t - x b_l)\Omega_r}}}{(1+x)(1+x\Lambda_3)}dx, \tag{25}$$

and

$$R_{x_t,erg}^{pSIC} = \frac{1}{2\ln 2}\int_0^{\frac{b_t}{b_l}} \frac{e^{-\frac{x}{\rho a_t \Omega_t} - \frac{x}{\rho(b_t - x b_l)\Omega_k} - \frac{x}{\rho(b_t - x b_l)\Omega_r}}}{1+x}dx, \tag{26}$$

respectively, where $\Lambda_3 = \frac{\varepsilon \Omega_I}{a_t \Omega_t}$ with $\varepsilon = 1$.

As can be seen from the above expressions, the exact analysis of ergodic rates require the computation of some complicated integrals. To facilitate these analysis and provide the simpler expression for the ergodic rate of x_t with ipSIC/pSIC, the following theorem and corollary provide the high SNR approximations to evaluate the performance.

Theorem 4. *The approximation expression for ergodic rate of x_t with ipSIC at high SNR is given by*

$$R_{x_t,\infty}^{ipSIC} = \frac{1}{2(1-\Lambda_3)\ln 2}\left[\ln\left(1+\frac{b_t}{b_l}\right) - \ln\left(1+\frac{b_t\Lambda_3}{b_l}\right)\right]. \tag{27}$$

Proof: See Appendix E. ■

Corollary 4. *For the special case with $\varepsilon = 0$, the ergodic rate of x_t for pSIC can be approximated at high SNR as*

$$R_{x_t,\infty}^{pSIC} = \frac{1}{2\ln 2}e^{\frac{1}{\rho a_t \Omega_t}}\left[\mathrm{Ei}\left(\frac{-1}{\rho a_t b_l \Omega_t}\right) - \mathrm{Ei}\left(\frac{-1}{\rho a_t \Omega_t}\right)\right]. \tag{28}$$

3) Slope Analysis: In this subsection, by the virtue of asymptotic results, we characterize the high SNR slope which is capable of capturing the influence of channel parameters on the ergodic rate. The high SNR slope is defined as

$$S = \lim_{\rho\to\infty}\frac{R_{x_i}^{\infty}(\rho)}{\log(\rho)}, \tag{29}$$

where $R_{x_i}^{\infty}$ denotes the asymptotic ergodic rate of x_i.

a) x_l for ipSIC/pSIC case:

Proposition 3. *Based on the above analytical results in* (22) *and* (23)*, when $\rho \to \infty$, by using $\mathrm{Ei}(-x) \approx \ln(x) + E_c$ [35, Eq. (8.212.1)] and $e^{-x} \approx 1 - x$, where E_c is the Euler constant, the asymptotic ergodic rates of x_l with ipSIC/pSIC in the high regime are given by*

$$R_{x_l,\infty}^{ipSIC} = \frac{-1}{2\ln 2}\left[A(1+\Psi)(\ln(\Psi)+E_c) + \frac{B}{\Lambda_1}\left(1+\frac{\Psi}{\Lambda_1}\right)\right. \\ \left. \times\left(\ln\left(\frac{\Psi}{\Lambda_1}\right)+E_c\right) + \frac{E_c}{\Lambda_2}\left(1+\frac{\Psi}{\Lambda_2}\right)\left(\ln\left(\frac{\Psi}{\Lambda_2}\right)+E_c\right)\right], \tag{30}$$

and

$$R_{x_l,\infty}^{pSIC} = \frac{-1}{2\ln 2}\left[A(1+\Psi)(\ln(\Psi)+E_c)\right. \\ \left. + \frac{E_c}{\Lambda_2}\left(1+\frac{\Psi}{\Lambda_2}\right)\left(\ln\left(\frac{\Psi}{\Lambda_2}\right)+E_c\right)\right], \tag{31}$$

respectively.

Substituting (30) *and* (31) *into* (29)*, we can see that the high SNR slopes of x_l with ipSIC/pSIC are equal to zeros.*

b) x_t for ipSIC/pSIC case: Similar to (30) and (31), substituting (27) and (23) into (29), we observe that the high SNR slopes of x_t with ipSIC/pSIC are also equal to zeros.

Remark 3. *The above analytical results demonstrate that even if there is no IS between both antennas at the relay, x_l and x_t converge to throughput ceilings and obtain zero slopes in the high SNR regime. This is due to the fact that the first phase is similar to uplink NOMA, it is suffering interference from other users which has seriously impact on the high SNR slope.*

4) Throughput Analysis: In delay-tolerant transmission scenario, the system throughput is determined by evaluating the ergodic rate. Based on the above results derived, the corresponding throughput of TWR-NOMA is given by

$$R_{dt}^{\psi} = R_{x_1,erg}^{\psi} + R_{x_2,erg}^{\psi} + R_{x_3,erg}^{\psi} + R_{x_4,erg}^{\psi}, \tag{32}$$

where $R_{x_1,erg}^{\psi}$ and $R_{x_3,erg}^{\psi}$ with ipSIC/PSIC can be obtained from (22) and (23), respectively, while $R_{x_2,erg}^{\psi}$ and $R_{x_4,erg}^{\psi}$ with ipSIC/pSIC can be obtained from and (25), (26), respectively.

V. ENERGY EFFICIENCY

In this section, the performance of TWR-NOMA systems is characterized from the perspective of energy efficiency (EE). In particular, EE has been adopted as a efficient metric to provide quantitative analysis for 5G networks. The core idea of EE is a rate between the total data rate of all NOMA users and the total energy consumption. Therefore, the expression of EE can be given by

$$\eta_{EE} = \frac{\text{Total data rate}}{\text{Total energy consumption}}. \tag{33}$$

TABLE I: Table of Parameters for Numerical Results

Monte Carlo simulations repeated	10^6 iterations
Power allocation coefficients of NOMA	$b_1 = b_3 = 0.2$ $b_2 = b_4 = 0.8$
Targeted data rates	$R_1 = R_3 = 0.1$ BPCU $R_2 = R_4 = 0.01$ BPCU
Pass loss exponent	$\alpha = 2$
The distance between R and D_1 or D_3	$d_1 = 2$ m
The distance between R and D_2 or D_4	$d_2 = 10$ m

Based on the throughput analysis in (III-4) and (IV-4), the EE of TWR-NOMA systems is given by

$$\eta_{\Upsilon}^{EE} = \frac{2R_{\Upsilon}^{\psi}}{TP_u + TP_r}, \tag{34}$$

where $\Upsilon \in (dt, dl)$ and T denotes transmission time of the entire communication process. η_{dl}^{EE} and η_{dt}^{EE} are the system energy efficiency in delay-limited transmission mode and delay-tolerant transmission mode, respectively.

VI. Numerical Results

In this section, numerical results are provide to substantiate the system performance and investigate the impact levels of IS on outage probability and ergodic rate for TWR-NOMA. Monte Carlo simulation parameters used are summarized in Table I, where BPCU is short for bit per channel use. Due to the reciprocity of channels between user groups (i.e., G_1 or G_2) and R, the outage behaviors and ergodic rates of x_1 and x_2 in G_1 are presented to illustrate availability of TWR-NOMA. Without loss of generality, the power allocation coefficients of x_1 and x_2 are set as $a_1 = 0.8$ and $a_2 = 0.2$, respectively. Ω_1 and Ω_2 are set to be $\Omega_1 = d_1^{-\alpha}$ and $\Omega_2 = d_2^{-\alpha}$, respectively. The performance of conventional TWR-OMA is shown as a benchmark for comparison, in which the total communication process can be finished in five slots. In the first slot, the user nodes in G_1, i,e, D_1 and D_2 sends signal x_1 and x_2 to R. Meanwhile, the user nodes in G_2, i,e, D_3 and D_4 sends signal x_3 and x_4 to R. After completing the exchange of information, R sends signal x_3 and x_4 to D_1 and D_2 in the second and third slots, respectively. Then R sends signal x_1 and x_2 to D_3 and D_4 in the fourth and fifth slots, respectively. Except power allocation coefficients, other simulation parameters of TWR-OMA is similar to that of TWR-NOMA. It is worth pointing out that the signals are transmitted at full power for TWR-OMA.

A. Outage Probability

Fig. 2 plots the outage probabilities of x_1 and x_2 with both ipSIC and pSIC versus SNR for simulation setting with $\varpi_1 = \varpi_2 = 0.01$ and $\Omega_I = -20$ dB. The solid and dashed curves represent the exact theoretical performance of x_1 and x_2 for both ipSIC and pSIC, corresponding to the results derived in (9), (10) and (12), (13), respectively. Apparently, the outage probability curves match perfectly with Monte Carlo simulation results. As can be observed from the figure, the outage behaviors of x_1 and x_2 for TWR-NOMA are superior to TWR-OMA in the low SNR regime. This is due to the fact that the influence of IS is not the dominant factor at low SNR. Hence in this scenario, NOMA systems should work as much as possible at low SNR regime, such as, the wide coverage in rural areas and cell edge scenarios. Another observation is that the pSIC is capable of enhancing the performance of NOMA compare to the ipSIC. In addition, the asymptotic curves of x_1 and x_2 with ipSIC/pSIC are plotted according to (15), (16) and (17), (18), respectively. It can be seen that the outage behaviors of x_1 and x_2 converge to the error floors in the high SNR regime. The reason can be explained that due to the impact of residual interference by the use of ipSIC, x_1 and x_2 result in zero diversity orders. Although the pSIC is carried out in TWR-NOMA system, x_1 and x_2 also obtain zero diversity orders. This is due to the fact that when the relay first detect the strongest signal in the first slot, it will suffer interference from the weaker signal. This process is similar to the uplink NOMA [36]. Additionally, this observation verifies the conclusion **Remark 1** in Section III.

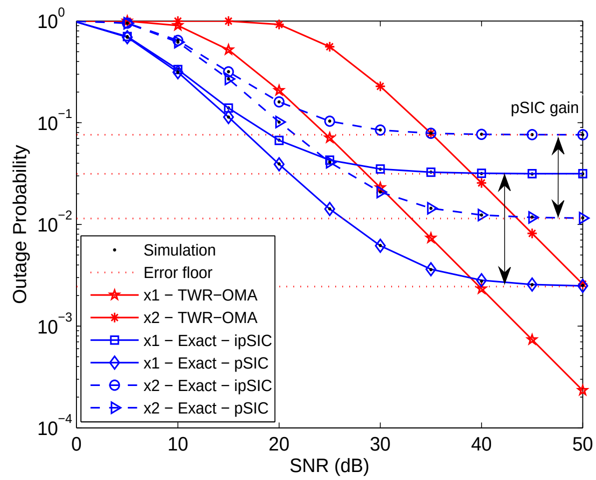

Fig. 2: Outage probability versus the transmit SNR, with $\varpi_1 = \varpi_2 = 0.01$, $R_1 = 0.1$, $R_2 = 0.01$ BPCU, and $\Omega_I = -20$ dB.

Fig. 3 plots the outage probabilities of x_1 and x_2 versus SNR with the different impact levels of IS from $\varpi_1 = \varpi_2 = 0$ to $\varpi_1 = \varpi_2 = 0.1$. The solid and dashed curves represent the outage behaviors of x_1 and x_2 with ipSIC/pSIC, respectively. As can be seen that when the impact level of IS is set to be $\varpi_1 = \varpi_2 = 0$, there is no IS between A_1 and A_2 at the relay, which can be viewed as a benchmark. Additionally, one can observed that with the impact levels of IS increasing, the outage performance of TWR-NOMA degrades significantly. As a consequence, it is crucial to hunt for efficient strategies for suppressing the effect of interference between antennas. Fig. 4 plots the outage probabilities versus SNR with different values of residual IS from -20 dB to 0 dB. It can be seen that the different values of residual IS affects the performance of ipSIC seriously. Similarly, as the values of residual IS increases, the preponderance of ipSIC is inexistent. When $\Omega_I = 0$ dB, the outage probabilities of x_1 and x_2 will be in close proximity to one. Therefore, it is important to design effective SIC schemes for TWR-NOMA.

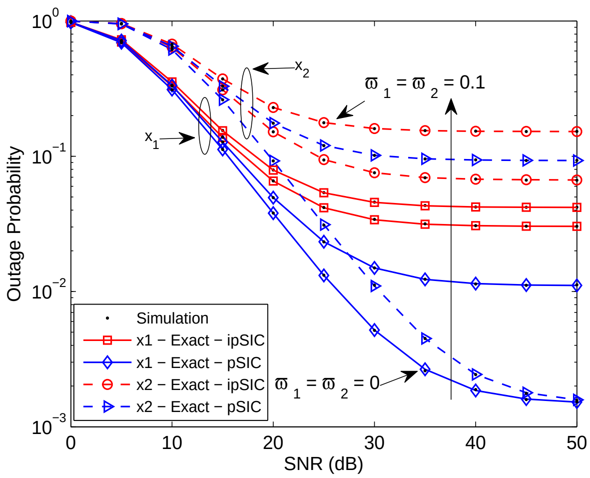

Fig. 3: Outage probability versus the transmit SNR, with the different impact levels of IS from $\varpi_1 = \varpi_2 = 0$ to $\varpi_1 = \varpi_2 = 0.1$, $R_1 = 0.1$, $R_2 = 0.01$ BPCU, and $\Omega_I = -20$ dB.

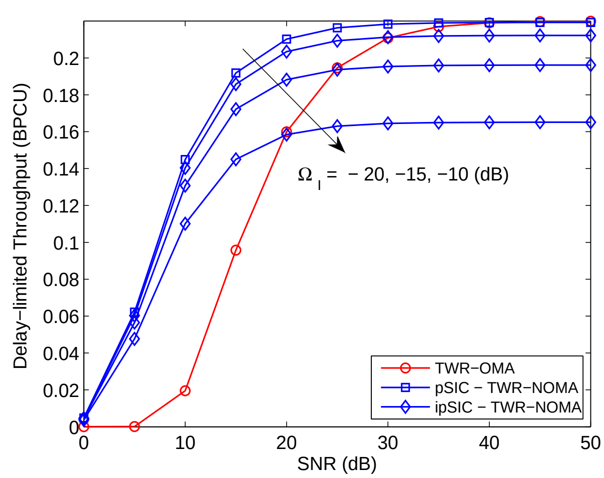

Fig. 5: System throughput in delay-limited transmission mode versus SNR with ipSIC/pSIC, $R_1 = 0.1$, $R_2 = 0.01$ BPCU, $\varpi_1 = \varpi_2 = 0.01$.

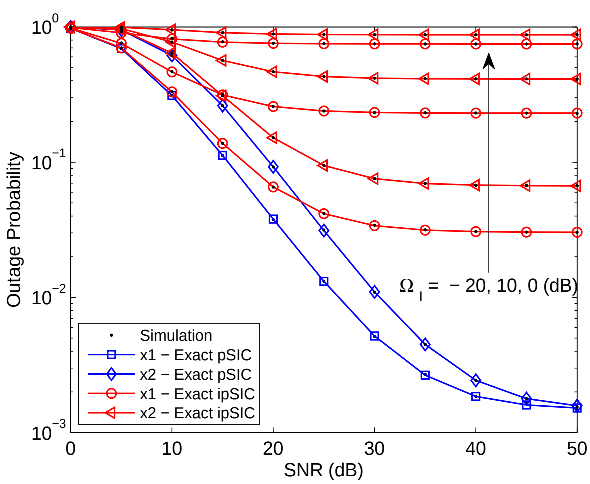

Fig. 4: Outage probability versus the transmit SNR, with different values of residual IS from -20 dB to 0 dB, $\varpi_1 = \varpi_2 = 0$, $R_1 = 0.1$, $R_2 = 0.01$ BPCU.

Fig. 5 plots system throughput versus SNR in delay-limited transmission mode for TWR-NOMA with different values of residual IS from -20 dB to -10 dB. The blue solid curves represent throughput for TWR-NOMA with both pSIC and ipSIC, which can be obtained from (19). One can observe that TWR-NOMA is capable of achieving a higher throughput compared to TWR-OMA in the low SNR regime, since it has a lower outage probability. Moreover, the figure confirms that TWR-NOMA converges to the throughput ceiling in the high SNR regime. Additionally, it is worth noting that ipSIC considered for TWR-NOMA will further degrade throughput with the values of residual IS becomes larger in high SNR regimes.

B. Ergodic Rate

Fig. 6 plots the ergodic rate of x_1 and x_2 for TWR-NOMA versus SNR and the values of SI are assumed to be $\varpi_1 = \varpi_2 = 0.01$, and $\Omega_I = -20$ dB. The blue and red dash-dotted curves represent the achievable rate of x_1 and x_2 with ipSIC/pSIC for TWR-NOMA, respectively, which considers IS between A_1 and A_2 at the relay. The blue and red solid curves represent ergodic rates of x_1 and x_2 with ipSIC/pSIC according to (22), (23) and (25), (26), respectively. We can observe that the ergodic rates of x_1 and x_2 with pSIC are larger than that of x_1 and x_2 with ipSIC. This is due to the fact that pSIC can provide more performance gain than ipSIC. In addition, due to the influence of interference, x_1 and x_2 converge to the throughput ceilings in high SNR regimes, which verifies the conclusion **Remark 3** in Section IV.

Fig. 7 plots the system throughput versus SNR in delay-tolerant transmission mode for TWR-NOMA. The blue solid curves represent system throughput for TWR-NOMA with ipSIC/pSIC, which can be obtained from (19). The system throughput of IS-based is selected to be the benchmark denoted by the red dash-dotted curves. It is observed that TWR-NOMA can achieve a higher throughput in the absence of IS at the relay. Hence, we need to find an effective way to restrain IS for both antennas at the relay.

C. Energy Efficiency

Fig. 8 plots energy efficiency of TWR-NOMA systems versus SNR with delay-limited/tolerant transmission modes. The red solid curves represent system energy efficiency for the delay-limited transmission mode with ipSIC/pSIC, respectively, which can be obtained from (19) and (34). The blue curves represent system energy efficiency for the delay-tolerant transmission mode with ipSIC/pSIC, respectively, which can be obtained from (32) and (34). It is can be seen that TWR-NOMA with ipSIC/pSIC in delay-limited transmission mode have almost the same energy efficiency. Additionally, we can

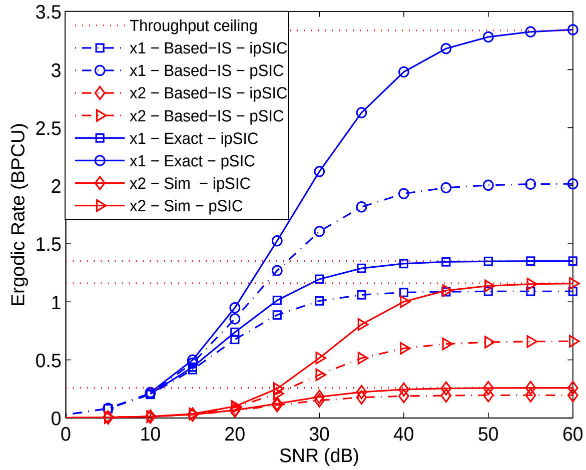

Fig. 6: Ergodic rate versus the transmit SNR with ipSIC/pSIC, $\varpi_1 = \varpi_2 = 0.01$, and $\Omega_I = -20$ dB.

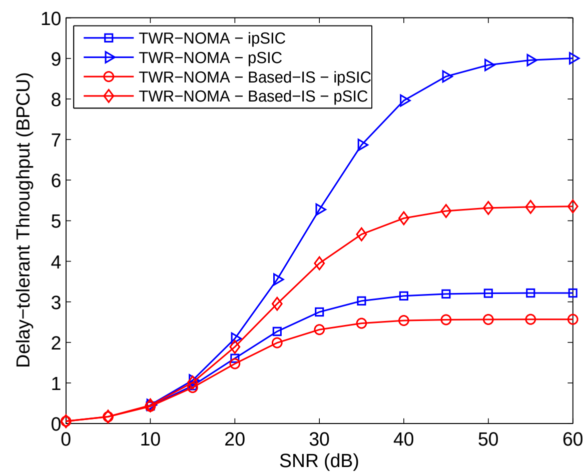

Fig. 7: System throughput in delay-tolerant transmission mode versus SNR with ipSIC/pSIC, $\varpi_1 = \varpi_2 = 0.01$, and $\Omega_I = -20$ dB.

observed that the energy efficiency of TWR-NOMA with pSIC is superior to ipSIC in high SNR regimes.

VII. Conclusion

This paper has investigated the application of TWR to NOMA systems, in which two pairs of users can exchange their information between each other by the virtue of a relay node. The performance of TWR-NOMA systems has been characterized in terms of outage probability and ergodic rate for both ipSIC and pSIC. The closed-form expressions of outage probability for the NOMA users' signals have been derived. Owing to the impact of IS at relay, there were the error floors for TWR-NOMA with ipSIC/pSIC in high SNR regimes and zero diversity orders were obtained. Based on the analytical results, it was shown that the performance of TWR-NOMA with ipSIC/pSIC outperforms TWR-OMA in the low

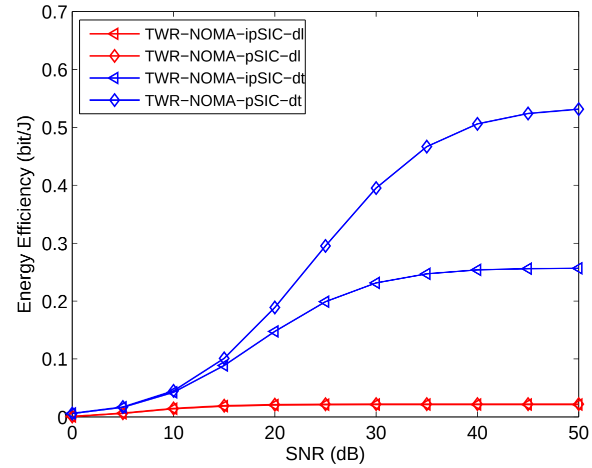

Fig. 8: System throughput in delay-limited/tolerant transmission mode versus SNR with ipSIC/pSIC, where $P_u = P_r = 10$ W, and $T = 1$.

SNR regime. Furthermore, the ergodic rates of TWR-NOMA have been discussed in detail. The results have shown that TWR-NOMA with pSIC is capable of achieving a larger rate in the absence of IS at the relay. More particularlly, the users' signals for TWR-NOMA converge to the throughput ceiling and gain zero high slopes in high SNR regimes. Finally, the system energy efficiencies with ipSIC/pSIC were discussed in a pair of transmission modes.

Appendix A: Proof of Theorem 1

Substituting (3), (5) and (6) into (8), the outage probability of x_l can be further given by

$$
\begin{aligned}
P_{x_l}^{ipSIC} = 1 & \\
& - \underbrace{\Pr\left(\frac{\rho |h_l|^2 a_l}{\rho |h_t|^2 a_t + \rho \varpi_1 (|h_k|^2 a_k + |h_r|^2 a_r) + 1} > \gamma_{th_l}\right)}_{J_1} \\
& \times \underbrace{\Pr\left(\frac{\rho |h_k|^2 b_t}{\rho |h_k|^2 b_l + \rho \varpi_2 |h_k|^2 + 1} > \gamma_{th_t}, \frac{\rho |h_k|^2 b_l}{\varepsilon \rho |g|^2 + \rho \varpi_2 |h_k|^2 + 1} > \gamma_{th_l}\right)}_{J_2}, \quad (A.1)
\end{aligned}
$$

where $\varepsilon = 1$.

To calculate the probability J_1 in (A.1), let $Z = \rho a_t |h_t|^2 + \rho \varpi_1 a_k |h_k|^2 + \rho \varpi_1 a_r |h_r|^2$. We first calculate the PDF of Z and then give the process derived of J_1. As is known, $|h_i|^2$ follows the exponential distribution with the parameters Ω_i, $i \in (1, 2, 3, 4)$. Furthermore, we denote that $Z_1 = \rho a_t |h_t|^2$, $Z_2 = \rho \varpi_1 a_k |h_k|^2$ and $Z_3 = \rho \varpi_1 a_r |h_r|^2$ are also independent exponentially distributed random variables (RVs) with parameters $\lambda_1 = \frac{1}{\rho a_t \Omega_t}$, $\lambda_2 = \frac{1}{\rho \varpi_1 a_k \Omega_k}$ and $\lambda_3 = \frac{1}{\rho \varpi_1 a_r \Omega_r}$, respectively.

Based on [37], for the independent non-identical distributed (i.n.d) fading scenario, the PDF of Z can be given by

$$f_Z(z) = \prod_{i=1}^{3} \lambda_i \left(\Phi_1 e^{-\lambda_1 z} - \Phi_2 e^{-\lambda_2 z} + \Phi_3 e^{-\lambda_3 z} \right), \quad \text{(A.2)}$$

where $\Phi_1 = \frac{1}{(\lambda_2-\lambda_1)(\lambda_3-\lambda_1)}$, $\Phi_2 = \frac{1}{(\lambda_3-\lambda_2)(\lambda_2-\lambda_1)}$ and $\Phi_3 = \frac{1}{(\lambda_3-\lambda_1)(\lambda_3-\lambda_2)}$.

According to the above explanations, J_1 is calculated as follows:

$$J_1 = \Pr\left(|h_l|^2 > (Z+1)\beta_l \right) = \int_0^\infty f_Z(z) e^{-\frac{(z+1)\beta_l}{\Omega_l}} dz, \quad \text{(A.3)}$$

where $\beta_l = \frac{\gamma_{th_l}}{\rho a_l}$. Substituting (A.2) into (A.3) and after some algebraic manipulations, J_1 is given by

$$J_1 = e^{-\frac{\beta_l}{\Omega_l}} \prod_{i=1}^{3} \lambda_i \left(\frac{\Phi_1 \Omega_l}{\Omega_l \lambda_1 + \beta_l} - \frac{\Phi_2 \Omega_l}{\Omega_l \lambda_2 + \beta_l} + \frac{\Phi_3 \Omega_l}{\Omega_l \lambda_3 + \beta_l} \right), \quad \text{(A.4)}$$

J_2 can be further calculated as follows:

$$\begin{aligned} J_2 &= \Pr\left(|h_k|^2 > \xi_t, |g|^2 < \frac{|h_k|^2 - \tau_l}{\varepsilon \rho \tau_l}, |h_k|^2 > \tau_l \right) \\ &= \Pr\left(|h_k|^2 > \max(\tau_l, \xi_t) \triangleq \theta_l, |g|^2 < \frac{|h_k|^2 - \tau_l}{\varepsilon \rho \tau_l} \right) \\ &= \int_\theta^\infty \frac{1}{\Omega_k} \left(e^{-\frac{y}{\Omega_k}} - e^{-\frac{y-\tau_l}{\varepsilon \tau_l \rho \Omega_I} - \frac{y}{\Omega_k}} \right) dy \\ &= e^{-\frac{\theta_l}{\Omega_k}} - \frac{\tau_l \varepsilon \rho \Omega_I}{\Omega_k + \varepsilon \rho \tau_l \Omega_I} e^{-\frac{\theta_l(\Omega_k + \rho \tau_l \varepsilon \Omega_I)}{\tau_l \varepsilon \rho \Omega_I \Omega_k} + \frac{1}{\varepsilon \rho \Omega_I}}, \end{aligned} \quad \text{(A.5)}$$

where $\xi_t = \frac{\gamma_{th_t}}{\rho\left(b_t - b_l \gamma_{th_t} - \varpi_2 \gamma_{th_t}\right)}$ with $b_t > (b_l + \varpi_2)\gamma_{th_t}$, $\tau_l = \frac{\gamma_{th_l}}{\rho\left(b_l - \varpi_2 \gamma_{th_l}\right)}$ with $b_l > \varpi_2 \gamma_{th_l}$.

Combining (A.4) and (A.5), we can obtain (9).

The proof is complete.

Appendix B: Proof of Theorem 2

Substituting (3), (4), (6) and (7) into (11), the outage probability of x_t is rewritten as

$$\begin{aligned} P_{x_t}^{ipSIC} &= 1 \\ &- \underbrace{\Pr\left(\frac{\rho |h_t|^2 a_t}{\varepsilon \rho |g|^2 + \rho \varpi_1 (|h_k|^2 a_k + |h_r|^2 a_r) + 1} > \gamma_{th_t}, \frac{\rho |h_l|^2 a_l}{\rho |h_t|^2 a_t + \rho \varpi_1 (|h_k|^2 a_k + |h_r|^2 a_r) + 1} > \gamma_{th_l} \right)}_{\Theta_1} \\ &\times \underbrace{\Pr\left(\frac{\rho |h_k|^2 b_t}{\rho |h_k|^2 b_l + \rho \varpi_2 |h_k|^2 + 1} > \gamma_{th_t} \right)}_{\Theta_2} \\ &\times \underbrace{\Pr\left(\frac{\rho |h_r|^2 b_t}{\rho |h_r|^2 b_l + \rho \varpi_2 |h_r|^2 + 1} > \gamma_{th_t} \right)}_{\Theta_3}, \end{aligned} \quad \text{(B.1)}$$

where $\varpi_1 = \varpi_2 \in [0,1]$ and $\varepsilon = 1$.

Similar to (A.2), let $Z' = \rho \varpi_1 a_k |h_k|^2 + \rho \varpi_1 a_r |h_r|^2$, the PDF of Z' is given by

$$f_{Z'}\left(z'\right) = \prod_{i=1}^{2} \lambda_i' \left(\frac{e^{-\lambda_1' z'}}{\left(\lambda_2' - \lambda_1'\right)} - \frac{e^{-\lambda_2' z'}}{\left(\lambda_2' - \lambda_1'\right)} \right), \quad \text{(B.2)}$$

where $\lambda_1' = \frac{1}{\rho \varpi_1 a_k \Omega_k}$ and $\lambda_2' = \frac{1}{\rho \varpi_1 a_r \Omega_r}$.

After some variable substitutions and manipulations,

$$\begin{aligned} \Theta_1 &= \Pr\left(|h_t|^2 > \beta_t \left(\varepsilon \rho |g|^2 + Z' + 1 \right), |h_l|^2 > \beta_l \left(\rho |h_t|^2 a_t + Z' + 1 \right) \right) \\ &= \int_0^\infty f_{Z'}\left(z'\right) e^{-\frac{\beta_l\left(z'+1\right)}{\Omega_l}} \times \int_0^\infty f_{|g|^2}(y) \frac{1}{\varphi_t \Omega_t} e^{-\beta_t\left(\varepsilon \rho y + z' + 1\right)\varphi_t} dy dz' \\ &= \frac{1}{\varphi_t \Omega_t \left(1 + \varepsilon \rho \beta_t \varphi_t \Omega_I\right)} e^{-\frac{\beta_l}{\Omega_1} - \beta_t \varphi_t} \times \int_0^\infty f_{Z'}\left(z'\right) e^{-\frac{\left(\beta_l + \beta_t \Omega_l \varphi_t\right) z'}{\Omega_l}} dz', \end{aligned} \quad \text{(B.3)}$$

where $\beta_t = \frac{\gamma_{th_t}}{\rho a_t}$ and $\varphi_t = \frac{\Omega_l + \rho \beta_l a_t \Omega_t}{\Omega_l \Omega_t}$.

Substituting (B.2) into (B.3), Θ_1 can be given by

$$\Theta_1 = \frac{e^{-\frac{\beta_l}{\Omega_l} - \beta_t \varphi_t}}{\varphi_t \Omega_t \left(1 + \beta_t \varepsilon \rho \varphi_t \Omega_I\right)\left(\lambda_2' - \lambda_1'\right)} \times \prod_{i=1}^{2} \lambda_i' \left(\frac{\Omega_l}{\beta_l + \beta_t \Omega_l \varphi_t + \Omega_l \lambda_1'} - \frac{\Omega_l}{\beta_l + \beta_t \Omega_l \varphi_t + \Omega_l \lambda_2'} \right). \quad \text{(B.4)}$$

Θ_2 and Θ_3 can be easily calculated

$$\Theta_2 = \Pr\left(|h_k|^2 > \xi_t \right) = e^{-\frac{\xi_t}{\Omega_k}}, \quad \text{(B.5)}$$

and

$$\Theta_3 = \Pr\left(|h_r|^2 > \xi_t \right) = e^{-\frac{\xi_t}{\Omega_r}}, \quad \text{(B.6)}$$

respectively, where $\xi_t = \frac{\gamma_{th_t}}{\rho\left(b_t - b_l \gamma_{th_t} - \varpi_2 \gamma_{th_t}\right)}$ with $b_t > (b_l + \varpi_2)\gamma_{th_t}$.

Finally, combining (B.4), (B.5) and (B.6), we can obtain (12) and the proof is completed.

Appendix C: Proof of Lemma 1

To derive the CDF F_X, based on (3) and (6), we can formulate

$$\begin{aligned} F_X(x) &= \Pr\left(\min\left(\frac{\rho |h_l|^2 a_l}{Z+1}, \frac{\rho |h_k|^2 b_l}{W+1} \right) < x \right), \\ &= \underbrace{\Pr\left(\frac{\rho |h_k|^2 b_l}{W+1} < \frac{\rho |h_l|^2 a_l}{Z+1}, \frac{\rho |h_k|^2 b_l}{W+1} < x \right)}_{Q_1} \\ &+ \underbrace{\Pr\left(\frac{\rho |h_l|^2 a_l}{Z+1} < \frac{\rho |h_k|^2 b_l}{W+1}, \frac{\rho |h_l|^2 a_l}{Z+1} < x \right)}_{Q_2}, \end{aligned} \quad \text{(C.1)}$$

where $Z = \rho a_t|h_w|^2 + \rho a_k\varpi_1|h_k|^2 + \rho a_r\varpi_1|h_r|^2$ and $W = \varepsilon\rho|g|^2 + \rho\varpi_2|h_k|^2$. For the i.n.d variable, based on (A.2) and (B.2), the PDF f_Z and f_W can be written as $f_Z(z) = \prod_{i=1}^{3}\lambda_i\left(\Phi_1 e^{-\lambda_1 z} - \Phi_2 e^{-\lambda_2 z} + \Phi_3 e^{-\lambda_3 z}\right)$ and $f_W(w) = \frac{\tilde{\lambda}_1\tilde{\lambda}_2}{\tilde{\lambda}_2-\tilde{\lambda}_1}\left(e^{-\tilde{\lambda}_1 w} - e^{-\tilde{\lambda}_2 w}\right)$, respectively, where $\tilde{\lambda}_1 = \frac{1}{\varepsilon\rho}$ and $\tilde{\lambda}_2 = \frac{1}{\rho\varpi_2}$.

Q_1 can be calculated as follows:

$$\begin{aligned} Q_1 &= \Pr\left(|h_l|^2 > \frac{|h_k|^2 b_l(Z+1)}{a_l(W+1)}, |h_k|^2 < \frac{x(W+1)}{\rho b_l}\right) \\ &= \int_0^\infty\int_0^\infty f_W(w) f_Z(z)\int_0^{\frac{x(w+1)}{\rho b_l}}\frac{e^{-u\varphi}}{\Omega_k}dudzdt \\ &= \int_0^\infty\int_0^\infty \frac{f_W(w) f_Z(z)}{\varphi\Omega_k}\left(1-e^{-\frac{x(w+1)\varphi}{\rho b_l}}\right)dzdw, \end{aligned} \tag{C.2}$$

where $\varphi = \frac{a_l(w+1)\Omega_l + b_l(z+1)\Omega_k}{a_l(w+1)\Omega_l\Omega_k}$.

Similar to (C.2), after some algebraic manipulations, Q_2 is given by

$$Q_2 = \int_0^\infty\int_0^\infty \frac{f_W(w) f_Z(z)}{\vartheta\Omega_l}\left(1-e^{-\frac{x(z+1)\vartheta}{\rho a_l}}\right)dzdw, \tag{C.3}$$

where $\vartheta = \frac{a_l(w+1)\Omega_l + b_l(z+1)\Omega_k}{b_l(z+1)\Omega_k\Omega_l}$.

Combine (C.2) and (C.3), we can obtain (20).

The proof is completed.

Appendix D: Proof of Theorem 3

The proof starts by substituting $\varpi_1 = \varpi_2 = 0$ into (21), the ergodic rate of x_l with ipSIC is given by

$$\begin{aligned} R_{x_l,erg}^{ipSIC} &= \frac{1}{2}\mathbb{E}\left[\log\left(1+\underbrace{\min\left(\frac{\rho|h_k|^2 b_l}{\varepsilon\rho|g|^2+1}, \frac{\rho|h_l|^2 a_l}{\rho|h_t|^2 a_t+1}\right)}_{U}\right)\right] \\ &= \frac{1}{2\ln 2}\int_0^\infty \frac{1-F_U(u)}{1+u}du, \end{aligned} \tag{D.1}$$

where $\varepsilon = 1$.

Applying some algebraic manipulations, the CDF of U can be given by

$$F_U(u) = 1 - \frac{e^{-u\Psi}}{(1+u\Lambda_1)(1+u\Lambda_2)}, \tag{D.2}$$

where $\Lambda_1 = \frac{\varepsilon\Omega_I}{b_l\Omega_k}$, $\Lambda_2 = \frac{a_t\Omega_t}{a_l\Omega_l}$ and $\Psi = \frac{a_l\Omega_l + b_l\Omega_l}{\rho a_l b_l\Omega_l\Omega_k}$.

Substituting (D.2) into (D.1), the ergodic rate of x_l with ipSIC can be further expressed as follows:

$$\begin{aligned} R_{x_l,erg}^{ipSIC} &= \frac{1}{2\ln 2}\int_0^\infty \frac{e^{-u\Psi}}{(1+u)(1+u\Lambda_1)(1+u\Lambda_2)}du \\ &= \frac{1}{2\ln 2}\int_0^\infty\left(\frac{Ae^{-u\Psi}}{1+u} + \frac{Be^{-u\Psi}}{1+u\Lambda_1} + \frac{Ce^{-u\Psi}}{1+u\Lambda_2}\right)du \\ &= \frac{-1}{2\ln 2}\left[Ae^{\Psi}\mathrm{Ei}(-\Psi) + \frac{Be^{\frac{\Psi}{\Lambda_1}}}{\Lambda_1}\mathrm{Ei}\left(\frac{-\Psi}{\Lambda_1}\right)\right. \\ &\quad \left. + \frac{Ce^{\frac{\Psi}{\Lambda_2}}}{\Lambda_2}\mathrm{Ei}\left(\frac{-\Psi}{\Lambda_2}\right)\right], \end{aligned} \tag{D.3}$$

where $A = \frac{1}{\Lambda_1\Lambda_2 - \Lambda_2 - \Lambda_1 + 1}$, $B = \frac{A(\Lambda_1 - \Lambda_1\Lambda_2) - \Lambda_1}{(\Lambda_2 - \Lambda_1)}$ and $C = 1 - A - B$; (D.3) can be obtained by using [35, Eq. (3.352.4)].

The proof is completed.

Appendix E: Proof of Theorem 4

We can rewrite (25) as follows:

$$R_{x_t,erg}^{ipSIC} = \frac{1}{2}\mathbb{E}\left[\log\left(1+\underbrace{\min\left(\begin{array}{c}\frac{\rho|h_t|^2 a_t}{\varepsilon\rho|g|^2+1}, \frac{\rho|h_k|^2 b_t}{\rho|h_k|^2 b_l+1}, \\ \frac{\rho|h_r|^2 b_t}{\rho|h_r|^2 b_l+1}\end{array}\right)}_{Q_1}\right)\right], \tag{E.1}$$

where $\varepsilon = 1$.

At high SNR regime, Q_1 can be approximated as

$$Q_1 \approx \underbrace{\min\left(\frac{|h_t|^2 a_t}{\varepsilon|g|^2}, \frac{b_t}{b_l}\right)}_{X}. \tag{E.2}$$

As such, the CDF of X in (E.2) can be given by

$$F_X(x) = 1 - \frac{1}{1+x\Lambda_3}, 0 < x < \frac{b_t}{b_l}, \tag{E.3}$$

where $\Lambda_3 = \frac{\varepsilon\Omega_I}{a_t\Omega_t}$. Substituting (E.3) into (E.1) and through some manipulations, the approximation solution for ergodic rate of x_t with ipSIC at the high SNR regime can be obtained in (27).

The proof is completed.

References

[1] X. Yue, Y. Liu, S. Kang, A. Nallanathan, and Y. Chen, "Outage performance of two-way relay non-orthogonal multiple access systems," in *Proc. IEEE International Commun. Conf. (ICC), accepted*, Kansas, USA, May. 2018.

[2] "3GPP TR 38.913: Study on scenarios and requirements for next generation access technologies."

[3] L. Dai, B. Wang, Y. Yuan, S. Han, C. l. I, and Z. Wang, "Non-orthogonal multiple access for 5G: solutions, challenges, opportunities, and future research trends," *IEEE Commun. Mag.*, vol. 53, no. 9, pp. 74–81, Sep. 2015.

[4] Z. Ding, Y. Liu, J. Choi, Q. Sun, M. Elkashlan, C. L. I, and H. V. Poor, "Application of non-orthogonal multiple access in LTE and 5G networks," *IEEE Commun. Mag.*, vol. 55, no. 2, pp. 185–191, Feb. 2017.

[5] Y. Cai, Z. Qin, F. Cui, G. Y. Li, and J. A. McCann, "Modulation and multiple access for 5G networks," 2017. [Online]. Available: http://arxiv.org/abs/1702.07673.

[6] T. M. Cover and J. A. Thomas, *Elements of information theory*, 6th ed., Wiley and Sons, New York, 1991.

[7] "3rd Generation Partnership Projet (3GPP), "Study on downlink multiuser superposition transmation for LTE (Release 13), TR36.859, "Mar. 2015."

[8] Z. Ding, Z. Yang, P. Fan, and H. V. Poor, "On the performance of non-orthogonal multiple access in 5G systems with randomly deployed users," *IEEE Signal Process. Lett.*, vol. 21, no. 12, pp. 1501–1505, Dec. 2014.

[9] Y. Liu, Z. Qin, M. Elkashlan, Y. Gao, and L. Hanzo, "Enhancing the physical layer security of non-orthogonal multiple access in large-scale networks," *IEEE Trans. Wireless Commun.*, vol. 16, no. 3, pp. 1656–1672, Mar. 2017.

[10] H. Haci, H. Zhu, and J. Wang, "Performance of non-orthogonal multiple access with a novel asynchronous interference cancellation technique," *IEEE Trans. Commun.*, vol. 65, no. 3, pp. 1319–1335, Mar. 2017.

[11] L. Lv, J. Chen, Q. Ni, and Z. Ding, "Design of cooperative non-orthogonal multicast cognitive multiple access for 5G systems: User scheduling and performance analysis," *IEEE Trans. Commun.*, vol. 65, no. 6, pp. 2641–2656, Jun. 2017.

[12] J. N. Laneman, D. N. C. Tse, and G. W. Wornell, “Cooperative diversity in wireless networks: Efficient protocols and outage behavior,” *IEEE Trans. Inf. Theory*, vol. 50, no. 12, pp. 3062–3080, Dec. 2004.

[13] Z. Ding, M. Peng, and H. V. Poor, “Cooperative non-orthogonal multiple access in 5G systems,” *IEEE Commun. Lett.*, vol. 19, no. 8, pp. 1462–1465, Aug. 2015.

[14] J. B. Kim and I. H. Lee, “Capacity analysis of cooperative relaying systems using non-orthogonal multiple access,” *IEEE Commun. Lett.*, vol. 19, no. 11, pp. 1949–1952, Nov. 2015.

[15] Y. Liu, Z. Ding, M. Elkashlan, and H. V. Poor, “Cooperative non-orthogonal multiple access with simultaneous wireless information and power transfer,” *IEEE J. Sel. Areas Commun.*, vol. 34, no. 4, pp. 938–953, Apr. 2016.

[16] J. Men, J. Ge, and C. Zhang, “Performance analysis of non-orthogonal multiple access for relaying networks over Nakagami-m fading channels,” *IEEE Trans. Veh. Technol.*, to appear in 2016.

[17] ——, “Performance analysis for downlink relaying aided non-orthogonal multiple access networks with imperfect CSI over Nakagami-m fading,” *IEEE Access*, to appear in 2016.

[18] C. Zhong and Z. Zhang, “Non-orthogonal multiple access with cooperative full-duplex relaying,” *IEEE Commun. Lett.*, vol. 20, no. 12, pp. 2478–2481, Dec. 2016.

[19] C. E. Shannon, “Two-way communication channels,” *in Proc. 4th Berkeley Symp. Math. Stat and Prob.*, vol. 1, pp. 611–644, 1961.

[20] Y. U. Jang and Y. H. Lee, “Performance analysis of user selection for multiuser two-way amplify-and-forward relay,” *IEEE Commun. Lett.*, vol. 14, no. 11, pp. 1086–1088, Nov. 2010.

[21] R. H. Y. Louie, Y. Li, and B. Vucetic, “Practical physical layer network coding for two-way relay channels: performance analysis and comparison,” *IEEE Trans. Wireless Commun.*, vol. 9, no. 2, pp. 764–777, Feb. 2010.

[22] A. Hyadi, M. Benjillali, and M. S. Alouini, “Outage performance of decode-and-forward in two-way relaying with outdated CSI,” *IEEE Trans. Veh. Technol.*, vol. 64, no. 12, pp. 5940–5947, Dec. 2015.

[23] C. Li, B. Xia, S. Shao, Z. Chen, and Y. Tang, “Multi-user scheduling of the full-duplex enabled two-way relay systems,” *IEEE Trans. Wireless Commun.*, vol. 16, no. 2, pp. 1094–1106, Feb. 2017.

[24] K. Song, B. Ji, Y. Huang, M. Xiao, and L. Yang, “Performance analysis of antenna selection in two-way relay networks,” *IEEE Trans. Signal Process.*, vol. 63, no. 10, pp. 2520–2532, May. 2015.

[25] Z. Zhang, Z. Ma, Z. Ding, M. Xiao, and G. K. Karagiannidis, “Full-duplex two-way and one-way relaying: Average rate, outage probability, and tradeoffs,” *IEEE Trans. Wireless Commun.*, vol. 15, no. 6, pp. 3920–3933, Jun. 2016.

[26] P. K. Sharma and P. K. Upadhyay, “Performance analysis of cooperative spectrum sharing with multiuser two-way relaying over fading channels,” *IEEE Trans. Veh. Technol.*, vol. 66, no. 2, pp. 1324–1333, Feb. 2017.

[27] Z. Ding, P. Fan, and H. V. Poor, “Impact of user pairing on 5G non-orthogonal multiple-access downlink transmissions,” *IEEE Trans. Veh. Technol.*, vol. 65, no. 8, pp. 6010–6023, Aug. 2016.

[28] Z. Ding, H. Dai, and H. V. Poor, “Relay selection for cooperative NOMA,” *IEEE Wireless Commun.*, vol. 5, no. 4, pp. 416–419, Aug. 2016.

[29] X. Yue, Y. Liu, S. Kang, A. Nallanathan, and Z. Ding, “Exploiting full/half-duplex user relaying in NOMA systems,” *IEEE Trans. Commun.*, to appear in 2017.

[30] H. Cui, M. Ma, L. Song, and B. Jiao, “Relay selection for two-way full duplex relay networks with amplify-and-forward protocol,” *IEEE Trans. Wireless Commun.*, vol. 13, no. 7, pp. 3768–3777, Jul. 2014.

[31] G. L. H. Chen and J. Cai, “Spectral-energy efficiency tradeoff in fullduplex two-way relay networks,” *IEEE Syst. J.*, no. 7, pp. 1–10, 2015.

[32] M. F. Kader, M. B. Shahab, and S. Y. Shin, “Exploiting non-orthogonal multiple access in cooperative relay sharing,” *IEEE Commun. Lett.*, to appear in 2017.

[33] Y. Liu, Z. Ding, M. Elkashlan, and J. Yuan, “Non-orthogonal multiple access in large-scale underlay cognitive radio networks,” *IEEE Trans. Veh. Technol.*, vol. 65, no. 12, pp. 10 152–10 157, Dec. 2016.

[34] A. A. Nasir, X. Zhou, S. Durrani, and R. A. Kennedy, “Relaying protocols for wireless energy harvesting and information processing,” *IEEE Trans. Wireless Commun.*, vol. 12, no. 7, pp. 3622–3636, Jul. 2013.

[35] I. S. Gradshteyn and I. M. Ryzhik, *Table of Integrals, Series and Products*, 6th ed. New York, NY, USA: Academic Press, 2000.

[36] H. Tabassum, E. Hossain, and J. Hossain, “Modeling and analysis of uplink non-orthogonal multiple access in large-scale cellular networks using poisson cluster processes,” *IEEE Trans. Commun.*, vol. 65, no. 8, pp. 3555–3570, Aug. 2017.

[37] S. Nadarajah, “A review of results on sums of random variables,” *Acta Appl. Math.*, vol. 103, no. 2, pp. 131–141, Sep. 2008.